

Current Biology, Volume 27

Supplemental Information

**Coordination of Orofacial Motor Actions
into Exploratory Behavior by Rat**

Anastasia Kurnikova, Jeffrey D. Moore, Song-Mao Liao, Martin Deschênes, and David Kleinfeld

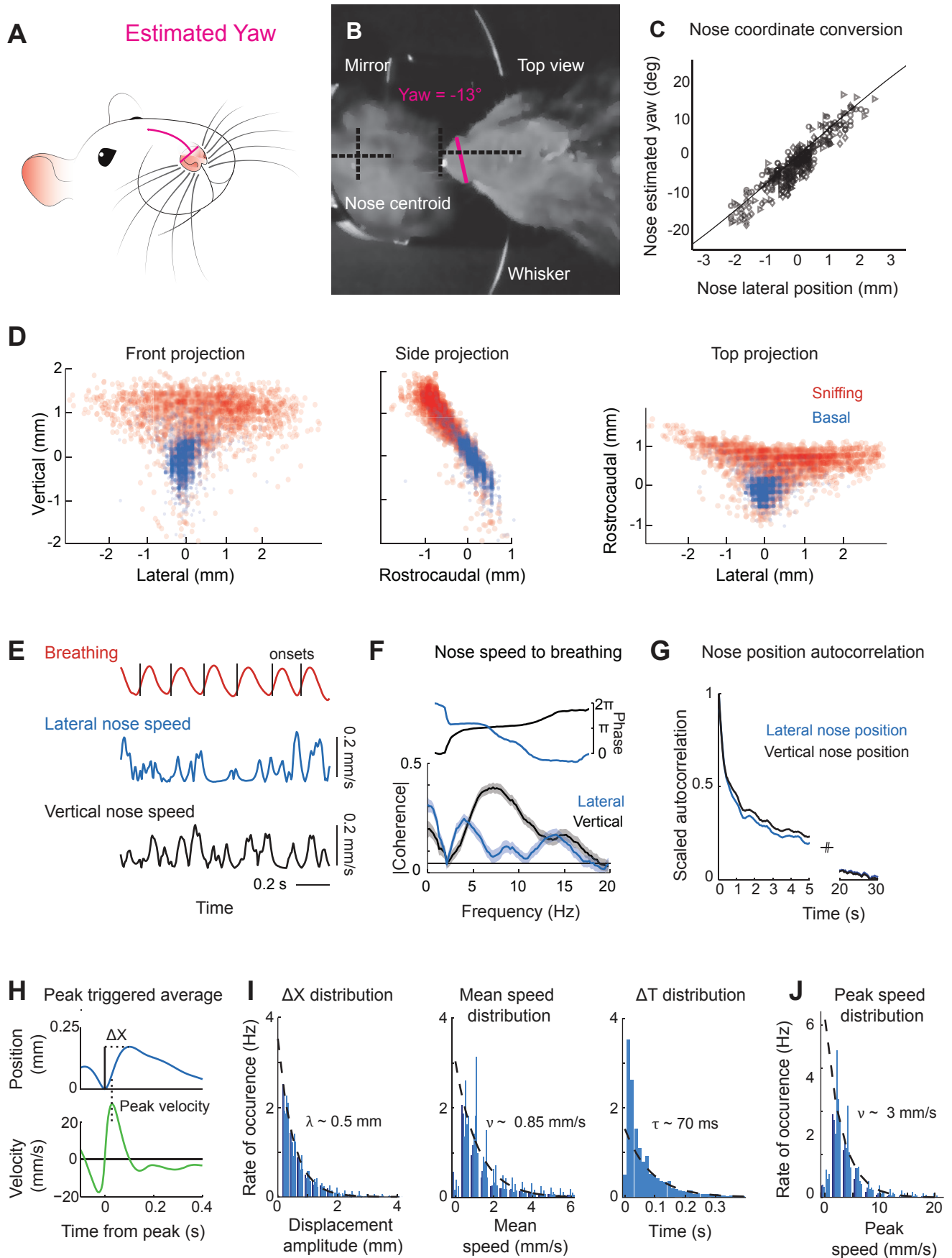


Figure S1

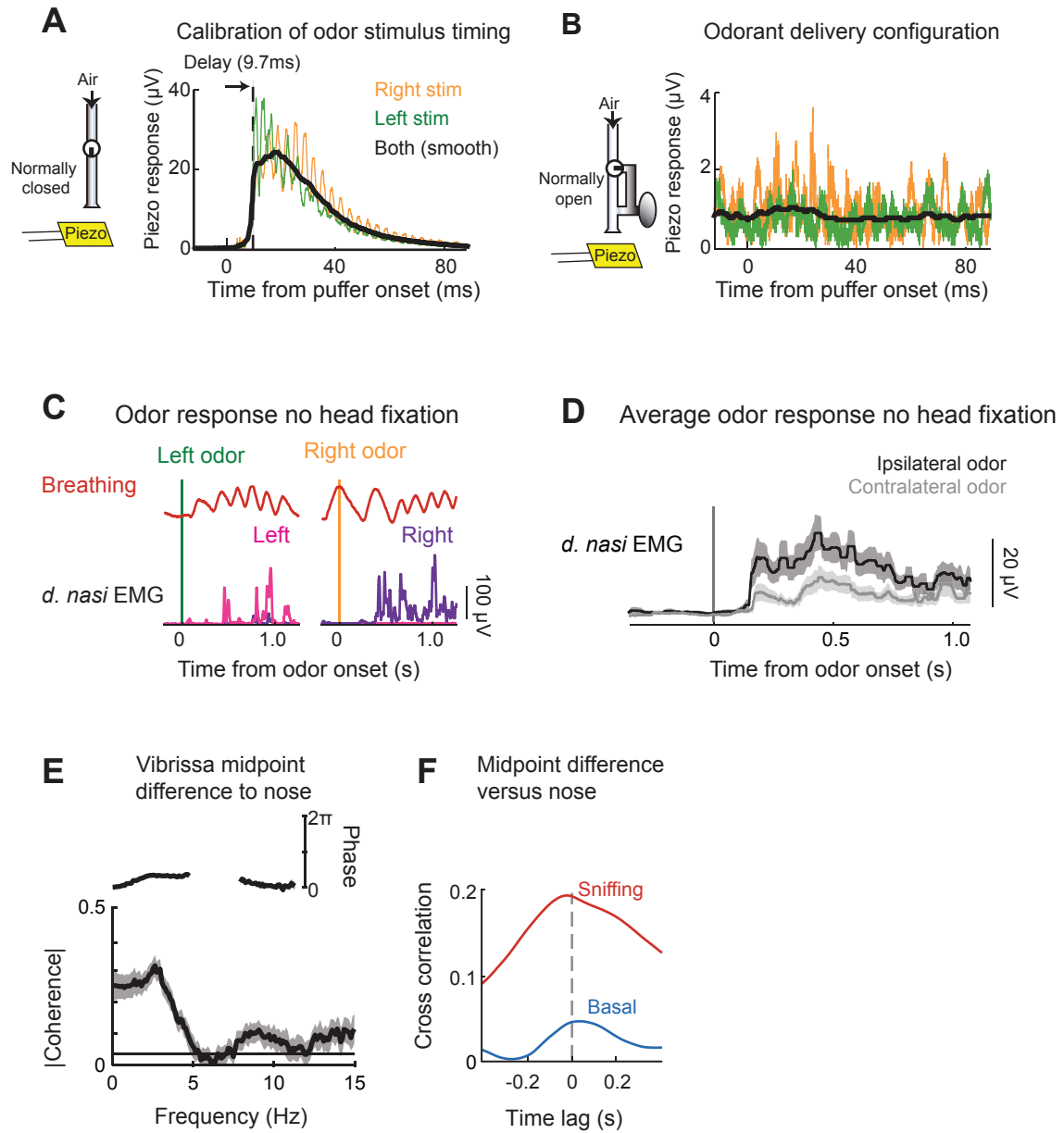


Figure S2

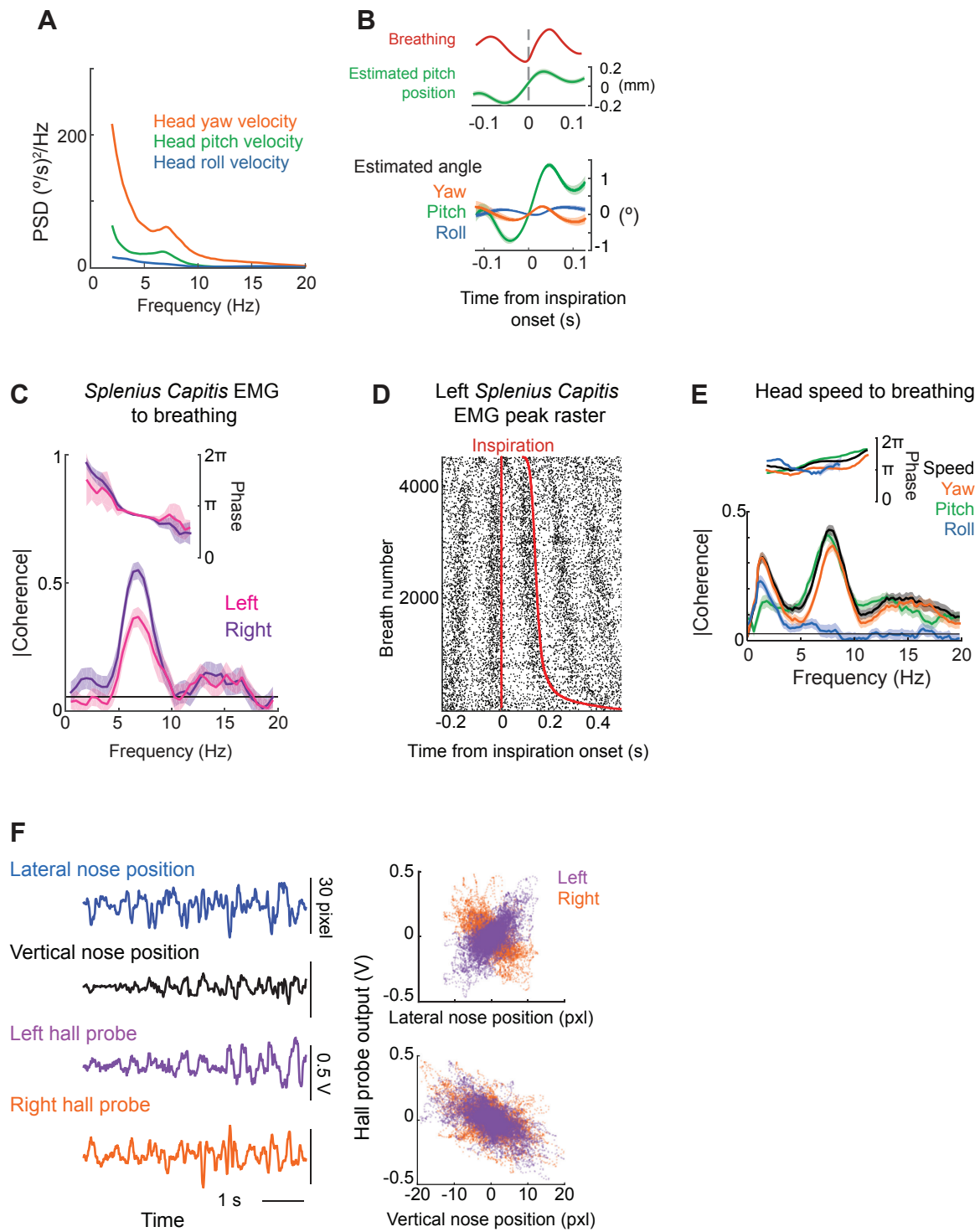


Figure S3

Figure S1: Motion of the nose; related to Figure 1.

(A) Diagram of estimated yaw (magenta).

(B) Example frame with nose deflected and yaw (magenta) tracked by hand as the angle between nostrils. Angle calculated as angle of the line. In the example Yaw = -13° .

(C) Example angles from 3 rats (square, circle, triangle) are tracked by hand as shown in yellow in panels B and C. Fit line shown is least squares fit to $\text{Yaw} = \arctan(\text{Position}/\text{Distance to Fulcrum})$. The effective fulcrum calculated from this fit is 7.6 mm caudal to the tip of the nose.

(D) 3D projections of histogram of nose positions. Front, Top and Side projections shown. Red dots show nose positions during sniffing (> 3 Hz respiration). Blue dots show nose positions during basal (< 3 Hz) respiration. The small rostrocaudal deflection correlates to the vertical motion, with $94 \pm 2\%$ of the variance of the three dimensional motion described by the two dominant principal components.

(E) Example 3 s clip of sniffing used to calculate coherence of nose velocities to breathing. Breathing is shown in red, with breath rises identified with black lines. Blue and black traces show the absolute value of the lateral and vertical velocities of nose motion.

(F) Coherence to breathing and phase of the lateral (blue) and vertical (black) velocities of nose movement during sniffing. The calculation was done on 3 s segments during which sniffing frequency was between 4 Hz and 8 Hz for a majority of the segment. Calculation performed with data from 3 animals.

(G) Scaled autocorrelation of lateral (blue) vertical (black) nose position. Autocorrelation for both drops to $\frac{1}{2}$ max at around 0.6 s, and reaches zero by 30 s.

(H) Average position (blue) and velocity (green) traces from each peak position in lateral nose motion. Velocity was calculated as the derivative of the spline fit to the position trace. Maximum displacement and peak velocity are indicated by dotted lines.

(I) Histograms of displacements between peaks in lateral motion and mean velocities between peaks for 6 rats (shades of blue), and histogram of times between peaks pooled across 6 rats. Black dotted line is an exponential fit to the histograms excluding values at less than 0.1 mm (displacement), 0.5 mm/s (velocity), and 30 ms (time).

Displacement fit is $\text{Rate} = 3.5 \exp(-\Delta x/0.5 \text{ mm})$, indicating a characteristic displacement of $\lambda = 0.5 \text{ mm}$.

Velocity fit is $\text{Rate} = 3.0 \exp(-\Delta v/0.9 \text{ mm/s})$, indicating a characteristic mean speed of $v = 0.9 \text{ mm/s}$

Time fit is $\text{Rate} = 1.5 \exp(-\Delta t/70 \text{ ms})$, indicating a characteristic speed of $\tau = 70 \text{ ms}$

(J) Histogram of peak velocities between peaks. Black dotted line is an exponential fit to the histograms excluding values near at less than 2 mm/s. Fit is $\text{Rate} = 8.3 \exp(-\Delta v/3.0 \text{ mm/s})$, indicating a characteristic speed of $v = 3 \text{ mm/s}$

Figure S2: Changes in the bias of deflection of the nose and vibrissae concurrent with odor presentation; related to Figure 3.

(A) Configuration of odor stimulator for timing test. Solenoid is configured such that at the time of stimulus presentation an air puff is delivered. A piezo-electric film placed at the distance of the nose is used to record average air flow after stimulus. Trace of piezo response to right (orange) and left (green) stimulus.

(B) Configuration of stimulator for odor test. Solenoid is configured such that at the time of stimulus presentation no air puff is delivered, and the air flow path changes such that the odorant is presented. With the same piezo-electric measurement as in panel C there is no apparent change in air flow at the time of stimulus presentation.

(C) Example trace of *d. nasi*. EMG envelope response to bedding odor presented laterally with the rat body restrained, but no head fixation. Right (purple) and left (magenta) *d. nasi* EMG envelopes and breathing signal are shown for a left (green) and right (orange) odor presentation. Each of the two sets of traces is from a single trial.

(D) Average response of the *d. nasi* EMG envelopes in the absence of head fixation, displayed relative to contra- (grey) versus ipsilateral (black) presentation of odorant. Data pooled over 29 presentations across 3 rats.

(E) Coherence of vibrissa midpoint asymmetry to nose is significant at low frequencies, with a phase near 0. Error is 95 % confidence intervals.

(F) Correlation of vibrissa midpoint difference to lateral nose position during sniffing epochs (red) and during all time (blue). Peak at 7 ms for sniffing trials (vibrissa asymmetry leading), and lower correlation during basal respiration. Cross correlations computed on 5 s segments during which breathing rate was over 3 Hz (sniffing) or under 2 Hz (basal). Data pooled across 3 rats.

Figure S3: Head bobbing and summary of rhythmic orofacial motor actions in relation to breathing; related to Figure 4.

(A) Power spectral density of head velocity during sniffing. Yaw (orange) pitch (green) and roll (blue) are calculated from accelerometer measurements. Calculation performed on same data as in part (A)

(B) Inspiration triggered average of breathing (red) and estimated pitch position (green) for sniffing, *i.e.*, > 4Hz breathing rate.

(C) Coherence between *Splenius Capitis* EMG envelope and inspiration onset during epochs of sniffing. Left EMG (magenta) and Right EMG (purple) are shown. Calculation performed with data from 1 animal.

(D) Raster plot of peaks in Left *Splenius Capitis* EMG envelope with respect to inspiration onset. Trials are sorted by breath duration. Data are from a single animal.

(E) Coherence between head speed and inspiration onset during epochs of sniffing. Calculations represent angular speed (black), yaw speed (orange) pitch speed (green) and roll speed (blue). Phase is head speed relative to inspiration onset times. The calculation was done on 3 s segments during which the sniffing frequency was between 4 Hz and 8 Hz for a majority of the segment. Calculation performed with data from 3 animals.

(F) Calibration between Hall-effect probe outputs and nose position from videography data in the head-restrained condition, example traces show lateral nose position (blue), vertical nose position (black), left hall probe output (purple), right hall probe output (orange). Correlation scatterplot of hall probe outputs to lateral and vertical nose position. Left (purple) hall probe is correlated with lateral position, while right (orange) is anti-correlated. Both outputs are anti-correlated with vertical position.

Supplemental experimental procedures

Subjects. Our data were collected from 25 Long Evans adult female rats, 250 to 350 g in mass. All experimental procedures on our animals were accordance with Guide for the Care and Use of Laboratory Animals and have been approved by Institutional Animal Care and Use Committee at University of California, San Diego.

Surgery. All surgeries were performed under ketamine (90 mg/kg rat mass) and xylazine (10 mg/kg rat mass) anesthesia. Injections were made intraperitoneally with supplemental injections of ketamine (20 mg/kg rat mass) given as needed. Buprenorphine, an analgesic agent, was administered after the surgery (20 μ l).

Video monitoring of nose and vibrissa position. Six Long Evans rats were implanted with a head post [S1] and a K-type thermocouple (5TC-TT-K-36-36, Omega Engineering) in the nasal cavity [S2]. Of these, one rat was implanted with two thermocouples, one in each nasal cavity. Rats were habituated to the head fixation rig after recovery as judged by normal grooming and whisking and a complete lack of struggling.

A high speed video camera (Basler A602f) was used to record nose and vibrissa motion at a rate of 216 fps, and spatial resolution of at least 170 μ m. A 45 degree mirror installed below the rat enabled tracking in all planes of motion. The tip of the nose and the C2 vibrissa on each side were marked using fabric paint (Tulip dimensional fabric paint, 65101) for tracking. To illuminate the rat for video, an 850 nm LED illuminator was used (Yr.seasons 48-LED Illuminator Light CCTV). Tracking was performed with custom software in Matlab either in real time, for just lateral and vertical movement of the nose, or *post hoc* from 60 s video segments for nose movement in three dimensions plus vibrissa tracking. First, we describe the distribution of nose positions in a head-restrained rat. **Figure 1A** shows a diagram of the setup for monitoring head-restrained nose motion and respiration.

Tracking of the vibrissae was performed as in past work [S3,S4]. The midpoint of whisking was calculated as the average of the rostral and caudal extrema in the position of the vibrissae.

We measure and report nose position in length, *i.e.*, millimeters. However, since air flow around the nostrils in rats is directed laterally [S5], lateral movement of the nose could also be interpreted as a change in angle between the nostrils. Thus we show a conversion to estimated angle for lateral motion (**Figure S1C**), with angle determined by manually marking the line between the nostrils in video frames. We fit a tangent function to the data to estimate the effective fulcrum, which we find to be 7.8 ± 0.4 mm caudal to the tip of the nose.

EMG recording. Thirteen rats were implanted with pairs of microwires in specific musculature and a

thermocouple in the nasal cavity. The targeted muscles were the left and right *d. nasi* in five rats; the left *d. nasi* only in one rat; the left and right *d. nasi* and the *nasolabialis* muscle in two rats; the left *d. nasi* and the left *nasolabialis* in two rats; and the left and right *splenius capitis* in three rats. Additionally, in three of the rats with microwires in *d. nasi*, microwires were also inserted acutely to target the intrinsic muscles of the pad immediately prior to a recording session.

For chronically implanted EMG recordings, 50 μm diameter perfluoroalkoxy insulated tungsten wire (AM systems 795500) was stripped 2-3 mm to form recording electrodes, and a 125 μm diameter PFA insulated tungsten wire (AM systems 796500) was stripped 4-5 mm for the reference electrode. Each wire was hooked and threaded through a 30 gauge needle. For measurements from *d. nasi*, an incision was made along the snout and the muscles exposed through a careful dissection of the overlying skin and fascia. Two or three recording electrodes were implanted in each muscle, and the reference electrode was placed along the snout. For measurements from *splenius capitis*, an incision was made along the midline in the back of the neck and the muscles exposed through a careful dissection of the overlying skin and fascia. Two recording electrodes were implanted in each muscle, and the reference electrode was placed below the scalp. In all cases, the wires were soldered to a custom board that was placed alongside the head plate and covered in Orthodontic Acrylic Resin (Ortho-Jet liquid and crystal powder, Lang Dental Manufacturing) to form a chronic implant. The EMG signals were acquired using a custom built amplifier [S6]. For the final measurement, the difference between the two spatially separated signals was formed, band pass filtered at between 300 Hz and 10 kHz with a zero-phase Butterworth filter, rectified, and finally low pass filtered at 50 Hz with a zero-phase Butterworth filter to extract the envelope of the muscle activity.

For acutely recording of mystacial EMGs, electrodes were prepared as for the chronic measurements. Rats were anesthetized with 3 % (v/v) isoflurane in 5 % (v/v) O₂, and recording electrodes were placed in the center of the C row by inserting the needle with the hooked electrode caudally to the pad and threading it to the desired location. The needles were then removed and the rats allowed to wake. The implant procedure took approximately two minutes. These EMG signals were acquired using a DAM 80 (World Precision Instruments) differential amplifier with the reference as ground.

Olfactory stimulation. We quantified nose motion in response to the controlled delivery of fumes from bedding of the home cage [S6,S7] (**Figure S2A,B**) alternately to the left or right nostril (**Figures 3A** and **S2C**). The deflection of the nose, along with the activation of the *d. nasi* muscles, was recorded in sessions that lasted no more than 30 minutes to minimize the effects of adaptation of behavior to the odorant.

A custom solenoid stimulator that flows air continuously to the nostrils, such that the air pressure does not change at the time of odor presentation, was constructed (**Figure 3A**). **Figure S2A-D** shows the calibration for the timing of the stimulator, reconfigured to deliver a puff of air, and a calibration for pressure change using a piezoelectric input, to show that air pressure does not change when odor is delivered. Odors are presented alternately to the left or right side at an interval between 25 and 250 s.

To block a nostril, we fill the naris with a minimal amount of silicone polymer. As confirmation that the nostril is blocked completely by this method, we compare breathing signals on the left and right side in a rat in which thermocouples are implanted in contralateral versus ipsilateral airways. We find that blocking one side completely abolished the breathing signal on that side (**Figure 3D**). In our subsequent analysis of trials, we exclude epochs where the rat is not following a normal breathing pattern, but rather chattering.

Gyrometer measurements. Three rats were implanted with a thermocouple and a mount for micro-electro-mechanical systems (MEMS) gyrometer sensors at least 2 days prior to behavioral testing. Immediately prior to behavioral testing the rats were manually restrained and connected to the MEMS gyrometer sensors, *i.e.*, yaw (LISY300ALST; Microelectronics) and pitch and roll (IDG-500; Invensens), and a miniature thermocouple pre-amplifier. Leads for both instruments were passed through a commutator [S6], amplified and low-pass filtered at 40 Hz. Rats were placed on a small, raised platform upon which where they were allowed to move and explore freely. They were periodically coaxed to sniff and whisk by presenting olfactory stimuli including the rat's home cage, bedding of another rat, or other odors [S6,S8]. The position of the rats was recorded simultaneously via an overhead webcam.

Magnetic sensor measurements. At least 2 days prior to behavioral monitoring, the rats were surgically implanted with a head restraint plate, a mount for a MEMS gyrometer, and two 4-40 screws atop the nasal bone as a mount for a custom-made, dual Hall-effect probe (no. A1389; Allegro Microsystems). Additionally, a small magnet, 2 to 5 mg in mass, was inserted into the nasal cartilage via an incision in the skin overlying the nasal bone. Prior to each behavioral session the rats were head restrained, the inertial sensor was mounted, and the Hall-effect probe was secured in place by affixing to the 4-40 screws with sandwiching nuts. While still head-restrained, the rats were coaxed to sniff, and nose position was monitored via high speed videography and via the magnetic sensors to verify placement of the magnet and that the output of the magnetic sensors reported nose position (**Figure S3F**).

Data Analysis. All routines were written in Matlab (The Mathworks); for spectra and coherence we used the Chronux routines [S9]. We confined our correlation and coherence analysis to sniffing

and basal breathing bouts of 3 s or more. We define the onset of an inspiration to be the rise time at which the amplitude of the signal reached 0.1-times the peak amplitude [S4]. We identified positive and negative directions of lateral nose motion when the amplitude of the motion exceeded 0.5 mm beyond the central position. For both lateral and vertical nose position, trials were split into left versus right motions and up versus down motion, respectively, to allow for averaging.

Supplemental references

- S1. Bermejo, R, Houben, D, and Zeigler, HP (1996) Conditioned whisking in the rat. *Somatosensory and Motor Research* 13:225-234.
- S2. Uchida, N and Mainen, ZF (2003) Speed and accuracy of olfactory discrimination in the rat. *Nature Neuroscience* 6:1224-1229.
- S3. Deschênes, M, Takato, J, Kurnikova, A, Moore, JD, Demers, M, Elbaz, M, Furuta, T, Wang, F, and Kleinfeld, D (2016) Inhibition, not excitation, drives rhythmic whisking. *Neuron* 90:374–387.
- S4. Moore*, JD, Deschênes*, M, Furuta, T, Huber, D, Smear, MC, Demers, M, and Kleinfeld, D (2013) Hierarchy of orofacial rhythms revealed through whisking and breathing. *Nature* 469:53-57.
- S5. Wilson, DA and Sullivan, RM (1999) Respiratory airflow pattern at the rat's snout and an hypothesis regarding its role in olfaction. *Physiology & Behavior* 66:41–44.
- S6. Ganguly, K and Kleinfeld, D (2004) Goal-directed whisking behavior increases phase-locking between vibrissa movement and electrical activity in primary sensory cortex in rat. *Proceedings of the National Academy of Sciences USA* 101:12348-12353.
- S7. Premack, D and Shanab, ME (1968) Rats prefer the home cage to the runway following intermittent but not consistent reinforcement. *Nature* 125:288-289.
- S8. Hill, DN, Curtis, JC, Moore, JD, and Kleinfeld, D (2011) Primary motor cortex reports efferent control of vibrissa position on multiple time scales. *Neuron* 72:344–356.
- S9. Mitra, PP and Bokil, HS, *Observed Brain Dynamics*. 2008, New York: Oxford University Press.